Broadband Photometric Reverberation Mapping with Meter-Class Telescopes

Carla June Carroll

A senior thesis submitted to the faculty of
Brigham Young University
in partial fulfillment of the requirements for the degree of

Bachelor of Science

Michael D. Joner, Advisor

Department of Physics and Astronomy

Brigham Young University

April 2013

ABSTRACT

Broadband Photometric Reverberation Mapping with Meter-Class Telescopes

Carla June Carroll
Department of Physics and Astronomy
Bachelor of Science

The environment surrounding supermassive black holes in active galaxies can be probed through the reverberation mapping technique. This technique requires the galactic nuclei to be simultaneously observed spectroscopically with a large 2m-class telescope and photometrically with a smaller telescope. Since obtaining large telescope time for long observing campaigns is difficult, we present a new broadband photometric reverberation mapping technique that can be performed on meter-class telescopes. Observations in the R and V band filters provide a measurement of time variable emission in Hα and Hβ respectively mixed with an observation of the continuum. The I band filter provides a continuum-only measurement. We obtained photometric observations in VRI on the 0.9-meter telescope at the West Mountain Observatory of the very broad-line Seyfert I galaxy Mrk 926 to test this technique. We found Mrk 926 relatively quiescent during the fall of 2012, though we originally selected Mrk 926 due to its strong emission lines and strong variability as described by Kollatschny & Zetzl (2010). This made estimation of Mrk 926's supermassive black hole mass impossible. Despite the quiescent results of Mrk 926, we produced high precision light curves from all filters over the period of several months. Our data are sufficient that had our target AGN been variable, we would have been able to measure delay times between the BLR and the nucleus.

Keywords: Mrk 926, Photometric Reverberation Mapping, West Mountain Observatory, BYU

ACKNOWLEDGMENTS

We acknowledge support from the BYU College of Physical and Mathematical Sciences as well as support from NSF Grant AST #0618209. This project also received funding through an ORCA grant. We also thank Dr. Van Huele and Dr. Moody of BYU faculty for assisting in the revisal and production of this thesis. A special thanks is given to Emily Ranquist for her aid in more efficient data analysis.

Contents

List of Figures

List of Tables

Chapter 1

Introduction

1.1 Statement of Problem

This thesis will address the question: Can we develop a method using our 0.9-m telescope that will allow an accurate estimate of the mass of a supermassive black hole through broadband photometric reverberation mapping? Other methods are available that accurately measure black hole mass, such as reverberation mapping, velocity outflow in radio and velocity dispersion. Each method is useful, e.g. velocity dispersions from radio and optical are more measures compared to the estimates from reverberation mapping. But these methods are tedious and expensive to implement. The area of a supermassive black hole and surrounding environment is so small compared to its host galaxy, that it cannot be resolved with any telescope. We decided to test out a possible broadband photometric reverberation mapping technique, which would make harnessing more information on supermassive black holes within active galaxies cheaper and more efficient.

Similar techniques have been recently probed theoretically as well as observationally (Chelouche & Daniel 2012; Chelouche et al. 2012; Edri et al. 2012; Haas et al. 2011; Nuñez et al. 2012). Based on Edri et al. (2012), we had high expectations for a positive result with Markarian

(Mrk) 926. Also, Kollatschny & Zetzl (2010) reported impressive variability and strong emission lines for Mrk 926 over a two-year period. This chapter will introduce vital concepts to understanding this method through topics on black hole mass (Sec. 1.2), Active Galactic Nuclei (Sec. 1.3), traditional reverberation mapping (Sec. 1.4) and broadband photometric reverberation mapping (Sec. 1.5). A review of our methods, results of Mrk 926, a discussion section identifying possibilities for explanation of the results and a conclusion are given later in the paper.

1.2 Black Hole Mass

Most if not all galactic nuclei contain supermassive black holes with $M > 10^6 M_\odot$. Whether these black holes originate through supernovae, collisions, mergers or other processes, it is generally accepted that each galaxy likely hosts a supermassive black hole in its nucleus. Because these nuclei are embedded in dense star fields, we know little about the details and structure of the regions surrounding them. Without this knowledge it is difficult to know anything about their formation and evolution.

Mass is one key link to this information and the most measurable characteristic of black holes. Mass estimates of black holes would provide greater empirical data to fit models of mass distribution throughout the universe and would bring insights into the foundations of quantum-gravity theories (Chelouche & Daniel 2012).

1.3 Active Galactic Nuclei

Active galaxies are defined as galaxies with an energy source in the central portion of the galaxy, or the bulge, that gives off radiation that cannot be attributed to stars. This radiation usually has a high energy tail that follows a power law with frequency. The energy is believed to derive from synchrotron emission associated with mass accreting onto a supermassive black hole within the

central region of the galaxy. This central region is known as the active galactic nucleus (AGN). They are generally compact, only lighthours or lightdays across, and in some cases would even be able to fit inside our solar system. Most galaxies are believed to contain supermassive black holes, but are classified as active if there exists material in the region of the black hole that can be accreted. Objects classified as AGNs include quasars, blazars, and Seyfert galaxies.

In the 1930s, Carl Seyfert found that about 10% of all galaxies had a bright, stellar-like source of their nucleus. The idea of AGN, or the idea that these compact regions inside an active galaxy are powered by accretion onto a supermassive black hole, was discussed first in the 1950s, but was not widely accepted at the time. Subsequent spectroscopic observations found that these nuclei contained broadened emission lines. In the 1960s identical broadened emission was found in stars, but displaced to high redshifts. These findings indicated that these objects were moving away from us at great speeds. These objects were later named quasi-stellar objects or quasars and distinguished as distant Seyfert galactic nuclei with higher luminosities.

The current model of AGNs could be compared to a bathroom sink, with the black hole as an infinite drain. As a sink drains dirty water (i.e. matter), a ring of material builds up near the drain (i.e. an accretion disk). This supposes that when matter falls onto the accretion disk (which consists of very fast moving gases), it is as if an unsuspecting particle meanders onto a race car track, colliding repeatedly with fast moving material and emitting high energy photons near the black hole. Thus, the accretion disk is the source of thermal continuum light.

This model for AGNs, shown in Fig. 1.1, exhibits the black hole at the center with a nearby accretion disk of fast moving matter. Near the accretion disk is the broad-line region (BLR), which contains fast moving gases ($v_{FWHM} > 800$ km/s) that cause Doppler broadening in the permitted lines, mainly of hydrogen. Previously, AGNs were classified on their spectral features, divided into blazars (variable high energy sources) and Seyferts. The unification model as seen in Fig. 1.1 clarifies that these sources are separate manifestations of the same structure with different possible

viewing angles. If viewing the jet end on, it is a blazar. At other angles, it is a Seyfert galaxy or quasar. Note that the Seyfert 1 viewing angle enables the viewer to see a good view of the BLR, which yields Doppler broadening of the broad-line region, whereas the Seyfert 2 view only provides a view of the narrow-line region, which yields Doppler broadening of the narrow-line region. In the narrow-line region, however, velocity measures do not give the kinematic information needed without the broadened emission lines. As seen in Fig. 1.1, the narrow-line region is a much greater distance from the black hole and at a much lower velocity.

Absolute magnitudes for AGNs can be on the order of $M_B = -23.5$ or $2.15 \times 10^{11} L_\odot$, making these objects the optically brightest in the observable universe. Variability is a distinguishing characteristic of AGNs. Their variability possibly comes from instabilities in the accretion disk, supernovae, starbursts, microlensing or other reasons not yet theorized. Optical flux changes occur on timescales of days. This rapid variability indicates the emitting source is extremely small.

To illustrate this, consider an instantaneous flash from a spherical object (as seen in Fig. 1.2). Light received from this burst would be "blurred" in time by an amount $\tau = R/c$ if the object is optically thick. The luminosity of Seyfert type AGNs commonly vary over days or hours, implying the broad-line source must be less than several light hours across. Reverberation mapping techniques assume the broad-line source is no larger than this.

1.4 Traditional Reverberation Mapping

Reverberation mapping was pioneered in the late 1990s and early 2000s (Peterson 2004). This technique assumes the standard model, and that AGNs follow the same relationship between black hole mass and host-galaxy bulge velocity dispersion (Merritt et al. 2001). Variability measures the radius of the broad-line region (Fig. 1.2). Solving the virial theorem for mass, $-2K = U$ (Carroll & Ostlie 1996), where U is the gravitational potential energy of the gas clouds in the broad-line

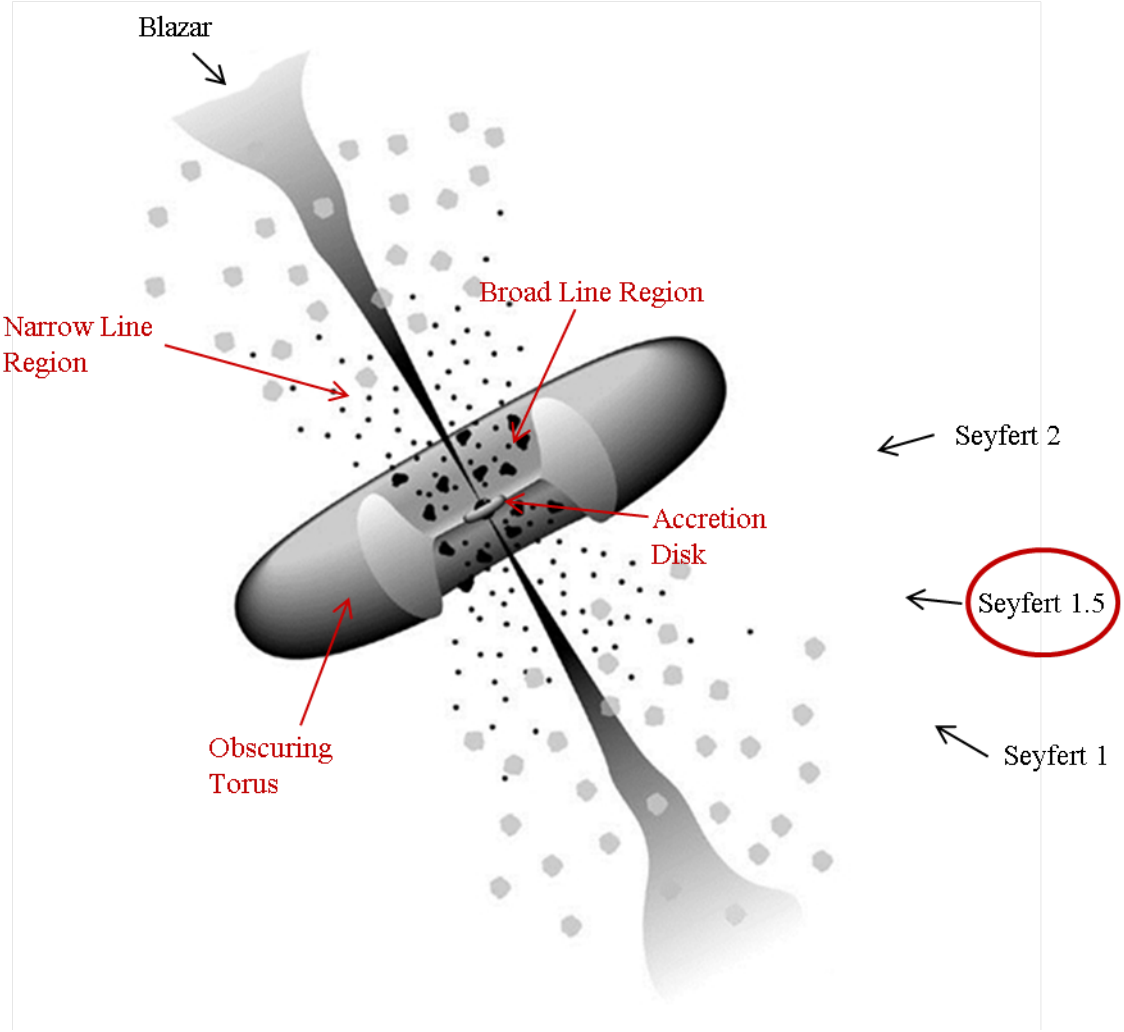

Figure 1.1 The Unification Model combines the different types of AGN into one explanation based on viewing angle. This model shows the black hole at the center with a nearby accretion disk of fast moving matter. Near the accretion disk is the broad-line region. Image adapted from Urry & Padovani (1995).

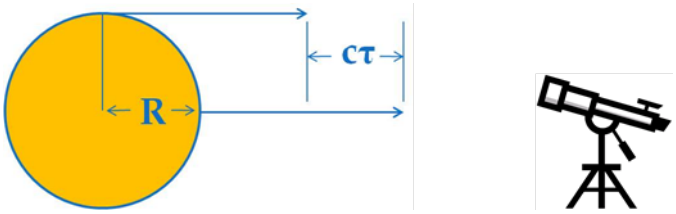

Figure 1.2 A spherical object of radius R emits an instantaneous flash of light, which is observed with a time lag τ=R/c. This method gives the radius of the broad-line region, $c\tau$, used in . The telescope represents the observer's viewing angle.

region, $U = -G\frac{M_{BH}m}{r_{BLR}}$ and K is the kinetic energy, $K = \frac{1}{2}m\Delta v^2$, where Δv is the velocity dispersion within the broad-line region. This yields a virial mass estimate,

$$M_{BH} = f\frac{\Delta v^2 c\tau}{G},$$

where f is a scaling factor, Δv is the Doppler broadening velocity, and $c\tau$ is the radius of the broad-line region as explained in section 1.3 and G is the gravitational constant.

Reverberation mapping requires spectroscopic data and imaging data. The imaging data give the variability of the AGN. This variability is not expected to be periodic, as is typical of many variable stellar sources. Rather, AGNs vary erratically by several tenths of a magnitude on time scales of hours, as explained in section 1.3. This variation is supposed to be due to new in-falling material onto the accretion disk or from instabilities in the magnetic field structure or from something yet unknown. Regardless of the source, a continuum brightening is followed by an increase in the broad-line emission flux with a lag of several days or weeks. We estimate the diameter of the broad-line region as $c\tau$.

Few ways exist to determine the supermassive black hole mass inside an AGN. One such method involves radio analysis of mass outflow of multiple Microwave Amplification by Stimulated Emission of Radiation (MASERs), which requires high spatial resolution. This method is very accurate, but requires the rare event of MASER occurrence within a galaxy near enough to resolve velocities. Reverberation mapping has been well accepted as another accurate method to

estimate black hole mass, though the need for spectroscopy requires telescopes of at least two meters in diameter. Such large telescopes are expensive to produce and require a long application process and a measure of luck. Such a process involves applying for time on the telescope and hoping that no weather, technical mishaps or other conditions stand in the way when/if time is granted. Because of this barrier, only ~50 AGNs have been reverberation mapped, giving a very small sample size for theorists to work with to use in gaining a better understanding of black hole characteristics and in probing dark energy (Haas et al. 2011; Watson et al. 2011).

1.5 Photometric Reverberation Mapping

Broadband photometric reverberation mapping is a new approach in modifying traditional reverberation mapping. It efficiently estimates the black hole mass, putting a greater weight on statistical analysis and less on spectral data. Narrowband photometric reverberation mapping is a similar method that accesses spectral features by only observing in a wavelength range that barely covers the spectral feature. However, each filter needs to be fit to the galaxy since galaxies have differing redshift. Filters are produced for one specific wavelength range, requiring multiple expensive filters for observations of objects with differing redshifts. Broadband photometric reverberation mapping covers more wavelength, using filters that are commonly accessible to universities and other organizations. The wavelengths covered are still able to extract the spectral feature's information as each broadband filter possesses only one dominant spectral feature.

The accuracy of broadband photometric reverberation mapping to photometric reverberation mapping is meticulously discussed by Chelouche & Daniel (2012). In this paper, they performed a feasibility study, based on numerical simulations, and found that line-to-continuum time delays associated with the BLR in AGNs can be deduced from broadband light curves. They applied their method to the Palomar-Green quasar sample, which had spectroscopic reverberation mapping

results for comparison. They found agreement between the accurate spectroscopic results and their photometric attempt.

Another example of broadband photometric reverberation mapping is from Edri et al. (2012). Edri et al. still used a lower luminosity source, allowing them to determine delays on the order of hours, instead of days or months using broadband photometric reverberation mapping. As seen in Fig. 2.1, features such as Hα at 6800 Å are dominant among the other features. If narrow filters are used, the capture of these filters is more accurate, though as there are no competing dominant features in each filter, broadband photometric data gives the same information in the variation of a specific spectral feature (e.g. Hα variations in the R filter will dominate R filter variation). These recent studies from Chelouche & Daniel (2012) and Edri et al. (2012) show that broadband photometric reverberation mapping provides a simplified observational approach to reverberation mapping without loss of accuracy.

Chapter 2

Methods

2.1 Observation Specifics

Observations were taken at Brigham Young University's West Mountain Observatory (WMO) with the f/5.5 0.91-meter Cassegrain telescope using the Fairchild 3041-UV (2k×2k) CCD, with plate scale 0.61"/pix. We determined exposure times based on the best seeing conditions for each night. We observed Mrk 926 on 49 nights between 03 August and 08 November 2012 and obtained 766 images in all filters. Images were taken with this CCD using the Johnson/Cousins V, R, and I filters as described in section 2.2. Mrk 926 was a high-priority observational target at WMO, and was thus observed every night that weather allowed.

2.2 Broadband Filter Set

We used the Johnson/Cousins broadband filter set V, R, and I. Historically, V stands for "Visible" with an effective wavelength (λ_{eff}) at 5510 Å and full width half maximum (bandwidth $\Delta\lambda$) at 880 Å. The R, or "Red", filter has an effective wavelength $\lambda_{eff} = 6580$ Å and bandwidth $\Delta\lambda = 1380$ Å. The I filter stands for "Infrared" though it is more accurately near-infrared with $\lambda_{eff} = 8060$ Å

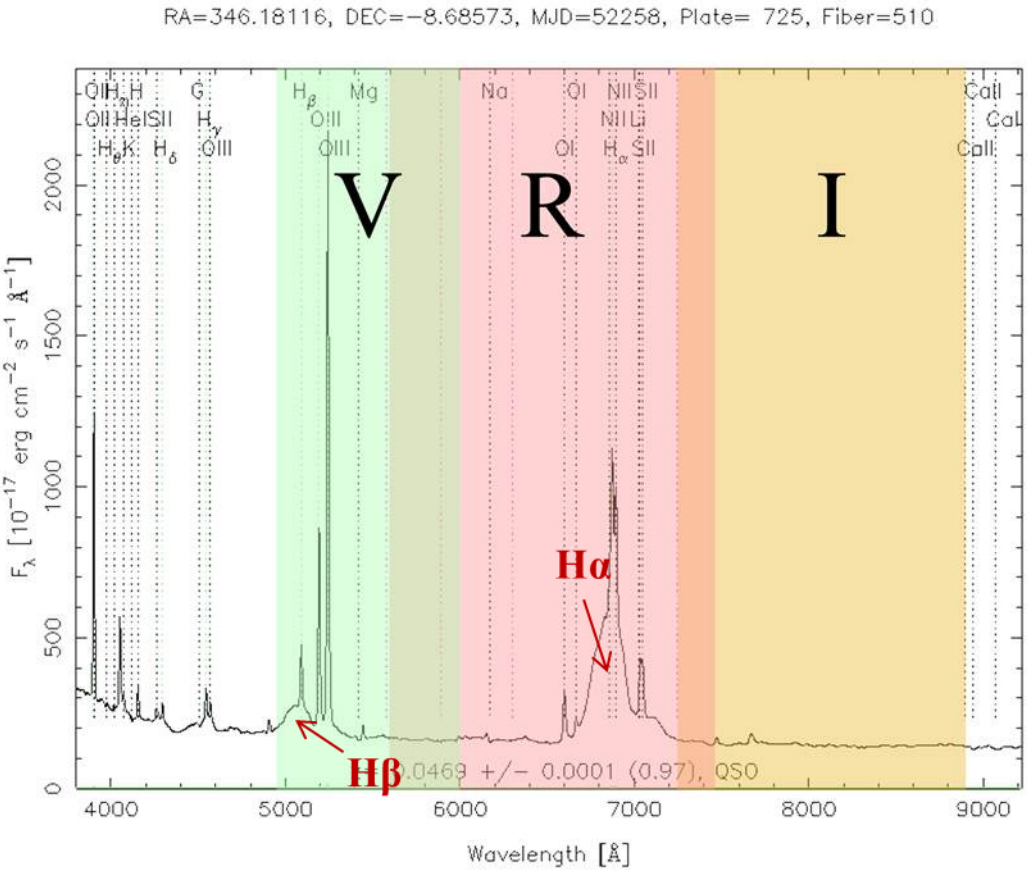

Figure 2.1 Broadband filters used at West Mountain Observatory (WMO) plotted on Sloan Digital Sky Survey (SDSS) spectra of galaxy Mrk 926. Wider filters (order 1000Å) such as these have not been used in reverberation mapping prior to 2012. The filters are: V (green), R (red), I (yellow). The y axis represents the flux F_λ and the x axis is the absorption wavelength in Å.

and bandwidth $\Delta\lambda = 1490$ Å. This is summarized in Table 2.1 and displayed in Fig. 2.1.

Reverberation mapping is based upon tracking the variability in emission lines of Hβ and Hα. The standard Johnson/Cousins V, R, and I superimposed onto the Sloan Digital Sky Survey (SDSS) emission spectra is shown in Fig. 2.1. In this figure, Hβ is the dominant permitted line in the V filter while Hα is the dominant permitted line within the R filter. Although OIII and NII are present in these filters, they are not created in the broad-line region and thus do not influence the broad-line variability. The I filter provides a continuum that will allow a cross-correlation function to

Table 2.1 Quantitative representation of Johnson/Cousins filter set in Fig. 2.1.

Filter	λ_{eff} [Å]	Bandwidth $\Delta\lambda$ [Å]	Description
V	5510	880	Visible
R	6580	1380	Red
I	8060	1490	Infrared

determine the time lag between a variation in Hβ (V filter) against that same variation seen in the continuum (I filter), as well as the time lag between a variation in Hα (R filter) against the continuum.

2.3 Image Reduction and Analysis Facility

We used the Image Reduction and Analysis Facility (IRAF) for all reductions of Mrk 926 to produce light curves as shown in Fig. 3.1. Images from WMO are taken raw and later reduced off-site. The standard process includes taking zero, dark, flat and object frames. Zero frames are taken with the shutter closed and zero exposure length. These frames enable correction for electron excitement in the CCD resulting from powering on the telescope. Zero frames are subtracted from dark frames, which are taken with an average exposure time expected for the night to correct for dead or hot pixels. The resulting product is divided from flat field frames, taken at sunset or sunrise to produce a zero gradient to correct for gradients resulting from imperfections in the CCD chip. Finally, the object frames of Mrk 926 divided out the corrected flat field frame, thus giving reduced data.

We performed aperture photometry within apphot, an analysis package in IRAF, on Mrk 926 to determine differential magnitudes. Aperture photometry subtracts the total photon count within an inner circular aperture fixed close to fit the point-spread function (PSF) of the star and an

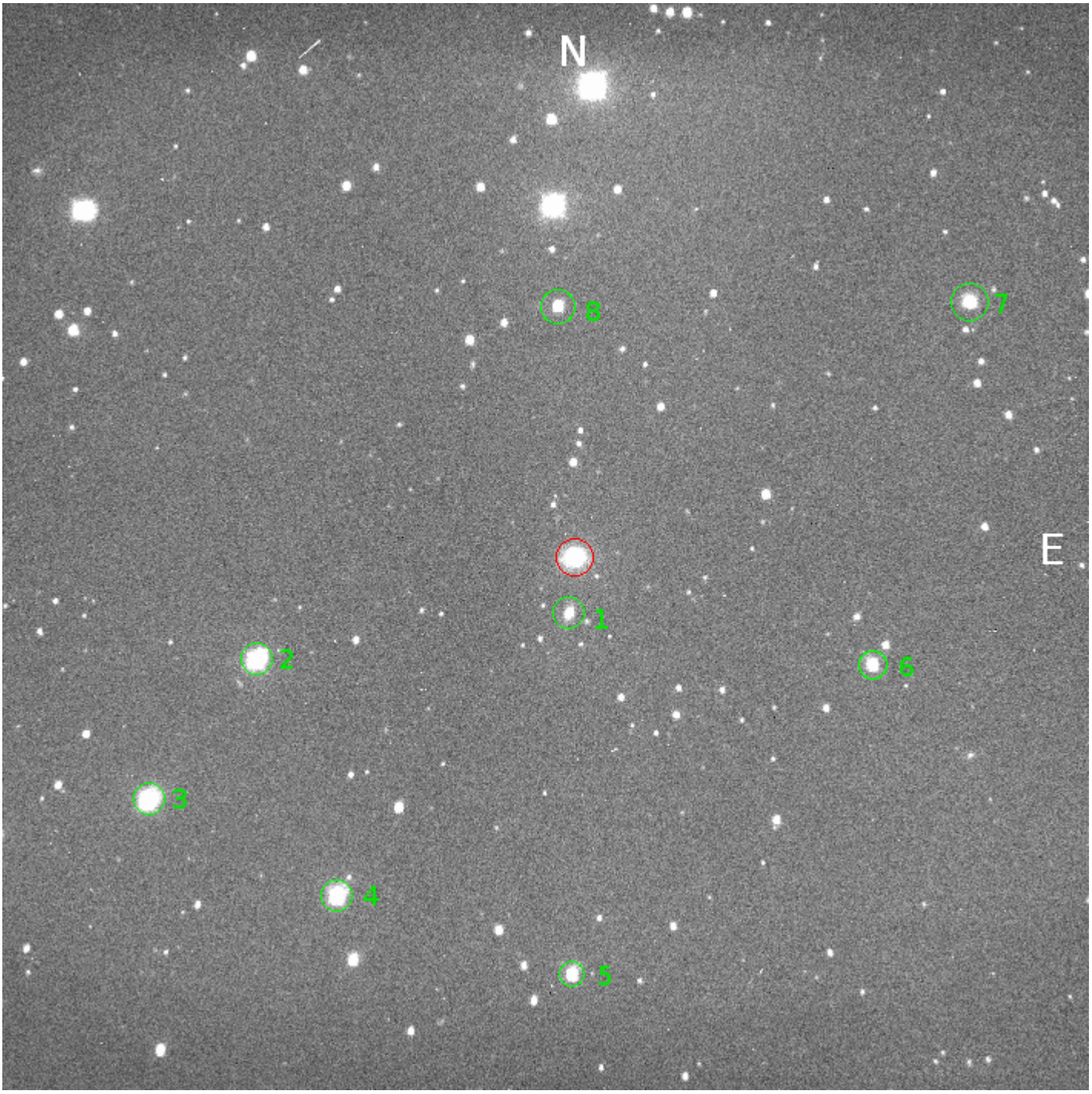

Figure 2.2 A typical image from WMO after basic processing. The red circle indicates the selected object, Mrk 926 and the green circles indicate the comparison stars. This example is from the V filter, though images from each filter vary insignificantly in appearance. This image has a 20.8' square field of view.

Table 2.2 Example of data in the V filter from 3 August 2012 (the first night of observations) produced after using apphot in IRAF. Errors were determined from the average counts for each object. The other eight stars listed besides Mrk 926 were used as comparison stars for differential analysis. For data from the other filters, see Tables 2.3 and 2.4.

Object	Instrumental Magnitude	Julian Date	Airmass	Error	Filter
Mrk 926	17.694	2456142.9195786	1.51718	0.012	V
Star 1	18.593	2456142.9195786	1.51718	0.026	V
Star 2	14.03	2456142.9195786	1.51718	0.001	V
Star 3	14.141	2456142.9195786	1.51718	0.001	V
Star 4	14.545	2456142.9195786	1.51718	0.001	V
Star 5	15.703	2456142.9195786	1.51718	0.002	V
Star 6	15.657	2456142.9195786	1.51718	0.002	V
Star 7	15.379	2456142.9195786	1.51718	0.002	V
Star 8	15.848	2456142.9195786	1.51718	0.003	V

outer circular aperture, which extends beyond the star's PSF representing the dark sky. Aperture photometry is done from the user's perspective by selecting objects (stars or point-like galaxies) in an image such as Fig. 2.2 while in IRAF. These quiescent stars serve as a baseline to allow a differential solution for the total inner photon counts in each star. A compilation of a sample of data produced in this process is shown in Tables 2.2, 2.3, and 2.4. With this data, we produce a differential solution using a program called varstar, which analyzes the variations in comparison stars and the target star. We used eight comparison stars and used an aperture size of six arc seconds, matching the average full width half max of Mrk 926's PSF.

Table 2.3 Example of data in the R filter from 3 August 2012 (the first night of observations) produced after using apphot in IRAF. Errors were determined from the average counts for each object. The other eight stars listed besides Mrk 926 were used as comparison stars for differential analysis. For data from the other filters, see Tables 2.2 and 2.4.

Object	Instrumental Magnitude	Julian Date	Airmass	Error	Filter
Mrk 926	16.917	2456142.92593308	1.522819	0.007	R
Star 1	17.775	2456142.92593308	1.522819	0.015	R
Star 2	13.539	2456142.92593308	1.522819	0.001	R
Star 3	13.643	2456142.92593308	1.522819	0.001	R
Star 4	14.075	2456142.92593308	1.522819	0.001	R
Star 5	15.118	2456142.92593308	1.522819	0.002	R
Star 6	15.144	2456142.92593308	1.522819	0.002	R
Star 7	14.748	2456142.92593308	1.522819	0.001	R
Star 8	15.199	2456142.92593308	1.522819	0.002	R

Table 2.4 Example of data in the I filter from 3 August 2012 (the first night of observations) produced after using apphot in IRAF. Errors were determined from the average counts for each object. The other eight stars listed besides Mrk 926 were used as comparison stars for differential analysis. For data from the other filters, see Tables 2.2 and 2.3.

Object	Instrumental Magnitude	Julian Date	Airmass	Error	Filter
Mrk 926	17.403	2456142.92415057	1.520951	0.009	I
Star 1	17.978	2456142.92415057	1.520951	0.014	I
Star 2	13.847	2456142.92415057	1.520951	0.001	I
Star 3	14.058	2456142.92415057	1.520951	0.001	I
Star 4	14.543	2456142.92415057	1.520951	0.001	I
Star 5	15.603	2456142.92415057	1.520951	0.002	I
Star 6	15.617	2456142.92415057	1.520951	0.002	I
Star 7	15.158	2456142.92415057	1.520951	0.002	I
Star 8	15.614	2456142.92415057	1.520951	0.002	I

Chapter 3

Results and Discussion

3.1 Review of Goal

Our idea for a broadband photometric reverberation mapping method for AGN at low redshift with meter-class telescopes requires two broadband filters containing Hα and Hβ with a third filter providing a pure continuum measurement. We were confident that this trial run would succeed in producing an accurate black hole mass estimate for Mrk 926, because Mrk 926 reportedly had strong variability and strong emission lines (Kollatschny & Zetzl 2010). Also, Edri et al. (2012) published a successful similar broadband photometric reverberation mapping attempt, though on a much larger telescope than meter-class. Thus, we observed Mrk 926 within the remaining observing season as a trial run and found Mrk 926 relatively quiescent during the time of our observations. We did secure precision of the measurements and compared to results of studies from other investigators (Chelouche & Daniel 2012), we expect exceptional results in the upcoming observing season.

3.2 Quiescence of Mrk 926

We found Mrk 926 remarkably quiescent (as seen in Fig. 3.1) during the fall of 2012 in comparison with its published results in 2010 (Kollatschny & Zetzl 2010). This section will discuss possible implications for this change in variability for Mrk 926.

Had we performed traditional reverberation mapping during the same time period for Mrk 926, we still would have found a quiescent result. To this point, we think we understand that variability is due to matter falling onto the accretion disk. If this situation fails to transpire, the AGN will appear as a normal galaxy, as it did in our case. Because spectral data required for traditional reverberation mapping requires a 2m class telescope, a quiescent result could still occur after all the effort and planning to acquire large telescope time. Broadband photometric reverberation mapping, however, makes the process available at the university level, where long-term observing projects can dictate telescope time. We do not know when an AGN will flare and thus cannot plan accordingly for projects, so a cheaper, easier method is needed from reverberation mapping to utilize time spent on these projects.

3.3 Accuracy

The light curve for another galaxy, observed at a similar time to Mrk 926 from WMO's 0.9 meter telescope, is plotted in Fig. 3.2. We expected to see variability on this scale, as opposed to the variability on the scale of 0.01 seen in Fig. 3.1. The scale of variability in Fig. 3.1 is too small for the telescope's capabilities to appropriately identify and perform a cross-correlation function, which is essential to reverberation mapping (Chelouche & Daniel 2012). We reject bad data processing as a viable argument for the quiescence of Mrk 926 based on other results from WMO such as the collaborative results from Luiyi et al. (2013) as seen in Fig. 3.2.

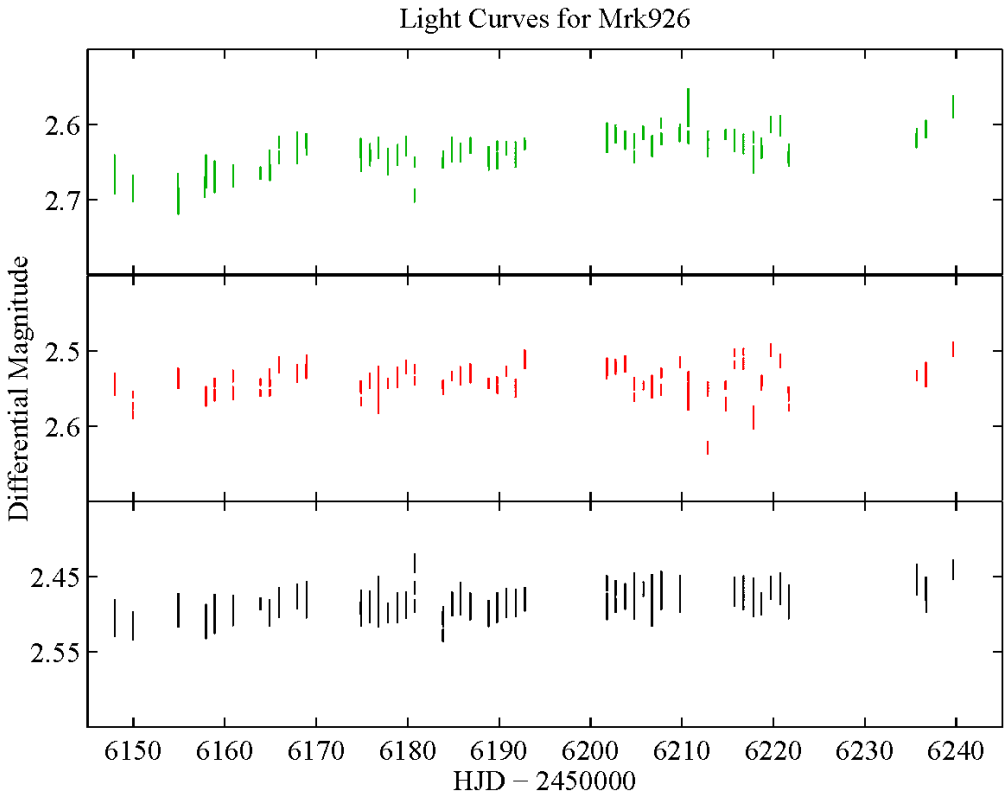

Figure 3.1 Mrk 926 light curves from WMO broadband filters V (top, green), R (middle, red) and I (bottom, black). The *x* axis is the Julian Date (in days). The *y* axis indicates the differential magnitude (mag) of Mrk 926 compared to several nonvariable stars around it. We expected significant variability in Mrk 926, but found less than 0.1 mag variability in each filter.

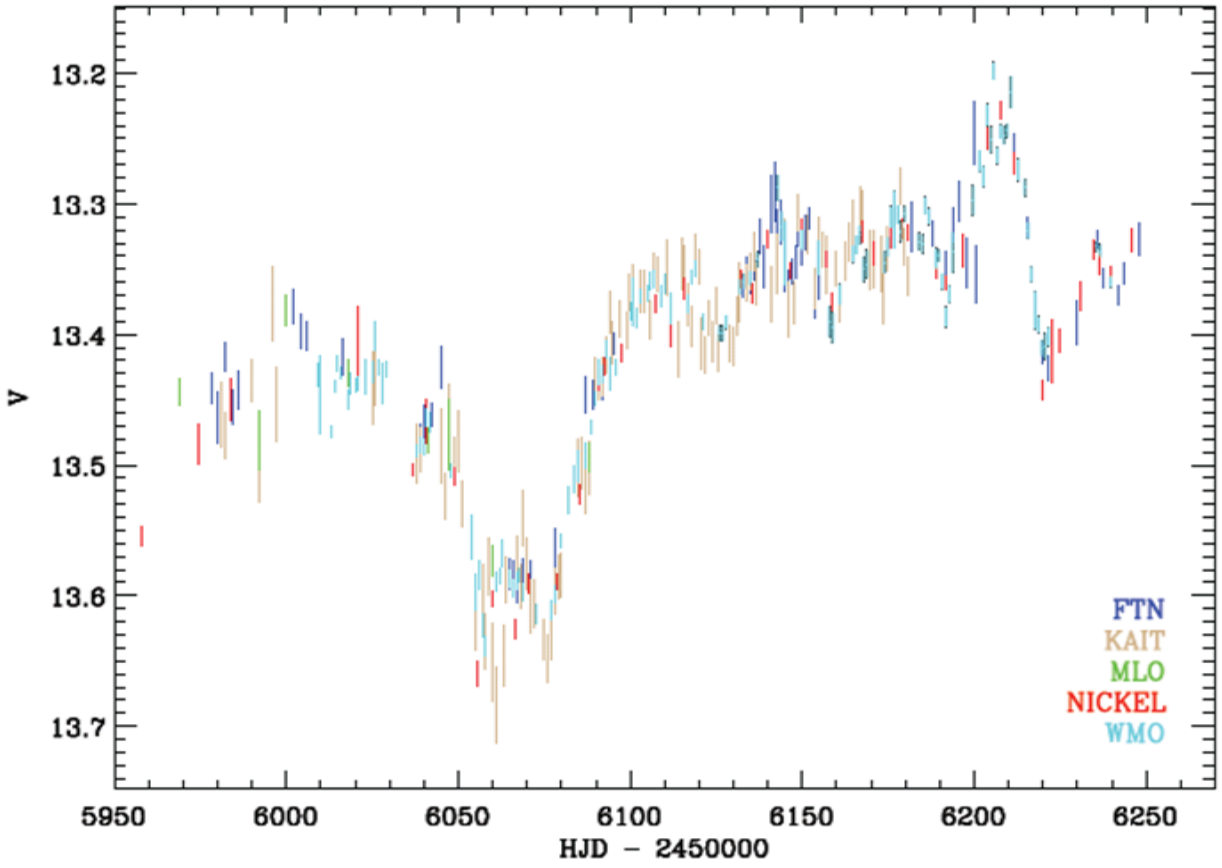

Figure 3.2 Light curve of K1858 from Pei et al. (Long Beach, CA, Jan. 2013) in collaboration with WMO. This light curve demonstrates variability on the order of about 0.5 magnitudes. We take this light curve as a good example of a typical expected light curve, emphasizing the quiescence of Mrk 926.

3.4 Suggestions for Further Work

We plan to observe three AGN starting Spring 2013, pursuing multiwavelength observations. We will carry out observations with support from a team at Lick Observatory, who will aid us in monitoring our selected objects spectroscopically. This will enable us to carefully check our photometric technique against reliably accurate results of traditional reverberation mapping. We will also observe these AGN at WMO using the 0.9 meter telescope, working with different filter combinations than were used in this study. If we are able to match these up with different broad emission line features in the AGN spectra, then we should be able to measure reverberation of various energy regions in the BLR. We will also pursue radio observations where possible with collaboration within the department at BYU.

Bibliography

Carroll, B. W., & Ostlie, D. A. 1996, An introduction to modern astrophysics, 1st edn. (Addison-Wesley Publishing Company, Inc.)

Chelouche, D., & Daniel, E. 2012, ApJ, 747, 62

Chelouche, D., Daniel, E., & Kaspi, S. 2012, ApJ, 750, 43

Edri, H., et al. 2012, ApJ, 756, 73

Haas, M., et al. 2011, ApJ, 535, 73

Kollatschny, W., & Zetzl, M. 2010, A&A, 522, 36

Merritt, D., Ferrarese, L., & Joseph, C. L. 2001, Science, 293, 1116

Nuñez, F. P., et al. 2012, A&A, 545, 84

Pei, L., et al. Long Beach, CA, Jan. 2013, presented at the 221st Meeting of the American Astronomical Society (AAS),

Peterson, B. M. 2004, IAU, 222, 6

Urry, C. M., & Padovani, P. 1995, ASP, 107, 803

Watson, D., Denney, K. D., Vestergaard, M., & Davis, T. M. 2011, ApJ, 740, 49

Index